Plant Cell Physiol. 44(12): 1290–1300 (2003)

Simultaneous Measurement of Stomatal Conductance, Non-photochemical Quenching, and Photochemical Yield of Photosystem II in Intact Leaves by Thermal and Chlorophyll Fluorescence Imaging

Kenji Omasa [1] and Kotaro Takayama

Department of Biological and Environmental Engineering, Graduate School of Agricultural and Life Sciences, The University of Tokyo, 1-1-1 Yayoi, Bunkyo, Tokyo, 113-8675 Japan

A new imaging system capable of simultaneously measuring stomatal conductance and fluorescence parameters, non-photochemical quenching (NPQ) and photochemical yield of photosystem II (Φ_{PSII}), in intact leaves under aerobic conditions by both thermal imaging and chlorophyll fluorescence imaging was developed. Changes in distributions of stomatal conductance and fluorescence parameters across *Phaseolus vulgaris* L. leaves induced by abscisic acid treatment were analyzed. A decrease in stomatal conductance expanded in all directions from the treatment site, then mainly spread along the lateral vein toward the leaf edge, depending on the ABA concentration gradient and the transpiration stream. The relationships between stomatal conductance and fluorescence parameters depended on the actinic light intensity, i.e. NPQ was greater and Φ_{PSII} was lower at high light intensity. The fluorescence parameters did not change, regardless of stomatal closure levels at a photosynthetically active photon flux (PPF) of 270 μmol m^{-2} s^{-1}; however, they drastically changed at PPF values of 350 and 700 μmol m^{-2} s^{-1}, when the total stomatal conductance decreased to less than 80 and 200 mmol m^{-2} s^{-1}, respectively. This study has, for the first time, quantitatively analyzed relationships between spatiotemporal variations in stomatal conductance and fluorescence parameters in intact leaves under aerobic conditions.

Keywords: Chlorophyll fluorescence imaging — Non-photochemical quenching — *Phaseolus vulgaris* L. — Photochemical yield of photosystem II — Stomatal conductance — Thermal imaging.

Abbreviations: ABA, abscisic acid; α_p, absorption coefficient of short-wavelength radiation by the leaf; D_H, thermal diffusivity in air; D_W, water vapor diffusivity in air; ε, emissivity of long-wavelength radiation of the leaf; E_s, short-wavelength radiation from the environment; E_w, long-wavelength radiation from the environment; ${}^iF$, fluorescence intensity image measured under actinic light; ${}^iF_m$, fluorescence intensity image measured during a saturation light pulse during darkness after exposure of the leaf to darkness for at least 1 h; ${}^iF_m'$, fluorescence intensity image measured during a saturation light pulse during steady-state photosynthesis; g_{aH}, boundary layer conductance to heat transfer; g_{aW}, boundary layer conductance to water vapor diffusion; g_{sl}, stomatal conductance to water vapor diffusion of the lower leaf surface; g_{st}, total stomatal conductance to water vapor diffusion; g_{su}, stomatal conductance to water vapor diffusion of the upper leaf surface; h, relative humidity of air; L, latent heat of evaporation; NPQ, non-photochemical quenching; PAR, photosynthetically active radiation; Φ_{PSII}, photochemical yield of photosystem II; PPF, photosynthetically active photon flux; PSI, photosystem I; PSII, photosystem II; ρc_p, volumetric heat capacity of air; σ, Stefan–Boltzmann constant; T_a, air temperature; T_l, leaf temperature; W, transpiration rate.

Introduction

Progress in imaging techniques now permits us to visualize spatiotemporal variations in invisible plant responses to various stresses, which cannot be detected by conventional point data measurements (e.g. Ellenson and Amundson 1982, Omasa et al. 1985, Omasa and Aiga 1987, Hashimoto et al. 1990, Omasa 1990, Kramer and Boyer 1995, Lichtenthaler et al. 1996, Chaerle and Straeten 2000, Govindjee and Nedbal 2000, Häder 2000, Omasa et al. 2002). In particular, at the level of an intact leaf, thermal imaging and chlorophyll fluorescence imaging techniques have been widely used to assess the dynamics and the heterogeneity of stomatal responses, called stomatal patchiness (Terashima et al. 1988, Terashima 1992, Beyschlag and Eckstein 1998), and the photosynthetic activity of the leaf surface.

Thermal imaging has often been used to remotely measure dynamic, heterogeneous distributions of leaf temperature, as a surrogate for direct measures of stomatal conductance (Horler et al. 1980, Omasa et al. 1980, Hashimoto et al. 1984, Omasa and Aiga 1987, Raskin and Ladyman 1988, Jones 1999). Stomatal conductance is an indicator of the extent of stomatal opening and indirectly indicates the rate of photosynthetic activity, i.e. CO_2 assimilation (Jones 1992). Recent studies have indicated the importance of quantitative evaluation of stomatal conductance from the measured leaf temperature and the basic energy-balance equation (Inoue et al. 1990, Taconet et al. 1995, Jones 1999). We previously reported that measuring the leaf temperature under strictly controlled environmental conditions allowed straightforward, quantitative evaluation of stomatal conductance to water vapor diffusion across the leaf surface (Omasa et al. 1981a, Omasa and Croxdale 1992). At

[1] Corresponding author: E-mail, aomasa@mail.ecc.u-tokyo.ac.jp; Fax, +81-3-5841-8175.

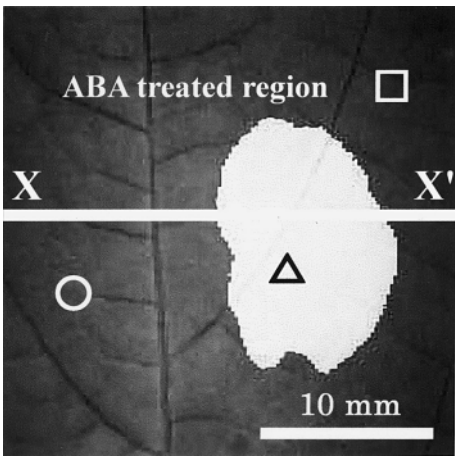

Fig. 1 Visual image of a measurement area of an attached *P. vulgaris* L. leaf used for the experiment performed at a PPF of 350 μmol m^{-2} s^{-1}. The white area represents an ABA-treated region, as determined by a superimposed thermal image obtained immediately after the ABA treatment. Symbols: the circle (site 1) is a mesophyll site separated by the midvein from the ABA-treated region, the triangle (site 2) represents the mesophyll site at the center of the ABA-treated region, and the square (site 3) represents a mesophyll site 6–7 mm away from the ABA-treated region along a lateral vein toward the leaf margin. Line X–X′ shows the profile analysis line used in the following analyses.

that time, this approach was applied only to an analysis of the effects of air pollutants on stomatal conductance (Omasa et al. 1981b, Omasa et al. 1981c).

Chlorophyll fluorescence results from absorbed light energy that was not used for photosynthetic reactions and heat dissipation. Chlorophyll fluorescence imaging provides information on photosynthetic activities without destruction of or contact with the living leaf (Omasa et al. 1987, Daley et al. 1989, Croxdale and Omasa 1990, Daley 1995, Rolfe and Scholes 1995, Lichtenthaler and Miehé 1997, Govindjee and Nedbal 2000, Omasa et al. 2002). Many useful fluorescence parameters, such as NPQ (non-photochemical quenching) and Φ_{PSII} (photochemical yield of photosystem II (PSII)), have been developed and used as proxies of photosynthetic activity under actinic light (Genty et al. 1989, Krause and Weis 1991, Govindjee 1995, Maxwell and Johnson 2000, Müller et al. 2001). An image of NPQ indicates the distribution and the strength of the intrathylakoid pH gradient and the ability of chloroplasts to dissipate excess excitation energy as heat on the leaf (Daley et al. 1989, Osmond et al. 1998, Müller et al. 2001). Therefore, NPQ images have been used as indicators of stomatal patchiness, because heat dissipation depends on stomatal closure (Daley et al. 1989, Mott 1995, Eckstein et al. 1996, Osmond et al. 1998). Φ_{PSII} images indicate the distribution of the yield of linear electron transport through PSII (Genty and Meyer 1995, Bro et al. 1996, Meyer and Genty 1998, Meyer and Genty 1999). Under anaerobic conditions, a Φ_{PSII} image can be used as a relative map of CO_2 assimilation and stomatal patchiness, because photorespiration and the Mehler reaction are completely inhibited under such conditions (Genty and Meyer 1995, Siebke and Weis 1995). Meyer and Genty (1998) demonstrated that quantitative calculation of stomatal conductance to water vapor diffusion on a leaf surface could be achieved with a Φ_{PSII} image measured under anaerobic conditions. However, the effects of anaerobic conditions on stomatal conductance and other photosynthetic activities are controversial (Osmond 1981, Ort and Baker 2002).

In this study, we therefore developed a new imaging system capable of concurrent, quantitative, straightforward evaluation of stomatal conductance, NPQ, and Φ_{PSII} in intact, attached leaves solely under aerobic conditions, by using both thermal imaging and chlorophyll fluorescence imaging. With this system, we quantitatively investigated relationships between spatiotemporal variations of stomatal conductance, NPQ, and Φ_{PSII} across intact *Phaseolus vulgaris* L. leaves in response to abscisic acid (ABA) treatment at individual small sites under three intensities of actinic light.

Results

Fig. 1 shows a visual image of *P. vulgaris* L. leaf within a 2.6×2.6 cm leaf area in the center of the 5×5 cm measurement window (see Materials and Methods) used for the experiment at a photosynthetically active photon flux (PPF) of 350 μmol m^{-2} s^{-1}. The white area represents an ABA-treated region, as determined by thermal imaging immediately after the ABA treatment.

Fig. 2 shows changes in the distribution of total stomatal conductance values within the same area as in Fig. 1 from 0 to 90 min after ABA treatment under illumination at a PPF of 350 μmol m^{-2} s^{-1}. The stomatal conductance values along line X–X′ (shown in Fig. 1) are represented below each image. Before ABA treatment, stomatal conductance was uniformly distributed in the mesophyll areas, with values ranging from 449 to 512 mmol m^{-2} s^{-1}, except in the immediate vicinities of the mid and lateral veins (Fig. 2A). Immediately after ABA treatment, stomatal conductance decreased within and around the ABA-treated region, and the area of decreased conductance spread laterally with time. The decrease in stomatal conductance at the center of the treated region (i.e. site 2 in Fig. 1) was especially strong. The conductance was 193 mmol m^{-2} s^{-1} after 15 min, 125 mmol m^{-2} s^{-1} after 30 min, and only 56 mmol m^{-2} s^{-1} after 50 min, after which the value stayed in the range 56 to 64 mmol m^{-2} s^{-1} (Fig. 3). The area of decreasing stomatal conductance expanded in all directions for 50 min after ABA treatment (Fig. 2B, C); subsequently, it spread mainly along the lateral vein toward the leaf edge between 50 and 90 min after treatment (Fig. 2C, D). At an interveinal mesophyll site (site 3 in Fig. 1) that was 6–7 mm away from the ABA-treated region toward the leaf edge along a lateral vein, stomatal conductance showed little change during the initial 30 min after treatment, but it gradually decreased to 305 mmol m^{-2} s^{-1} at 60 min and

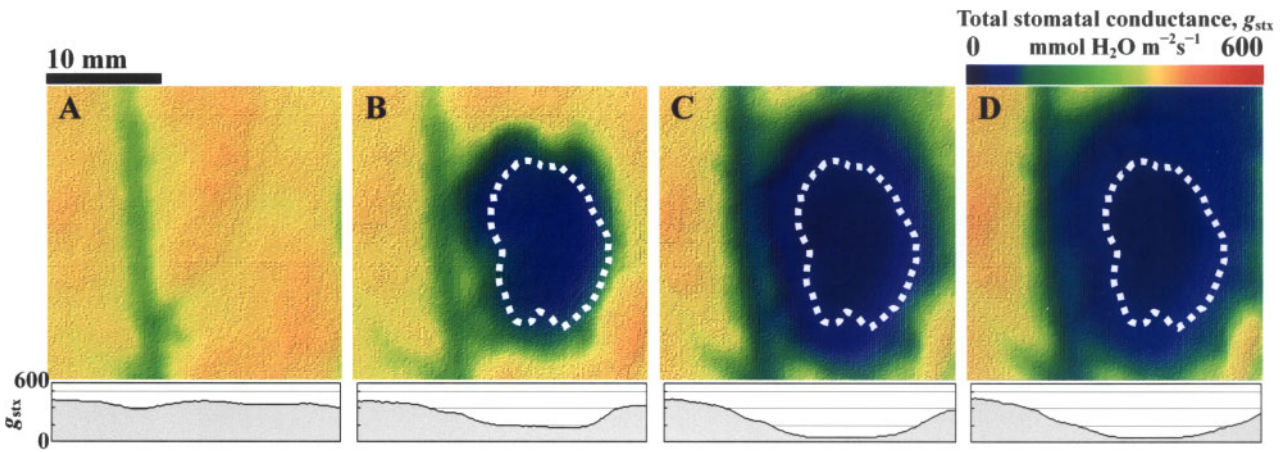

Fig. 2 Changes in the distribution of total stomatal conductance values (indicated by color) in the measurement area shown in Fig. 1 from 0 to 90 min after ABA treatment. The cross-sectional diagrams represent transects of total stomatal conductance values across the total stomatal conductance images along the line X–X′ shown in Fig. 1. The region within the dotted line (B–D) is the ABA-treated region. Experimental conditions were as follows: air temperature, 26.5°C; relative humidity, 48%; short-wavelength radiation, 44.5 W m^{-2}; long-wavelength radiation, 0.98 kW m^{-2}; actinic light intensity, PPF = 350 µmol m^{-2} s^{-1}; and boundary-layer conductance for heat transfer, 12.0 mm s^{-1}. (A) Just before ABA treatment; (B) 15 min after treatment; (C) 50 min after treatment; (D) 90 min after treatment.

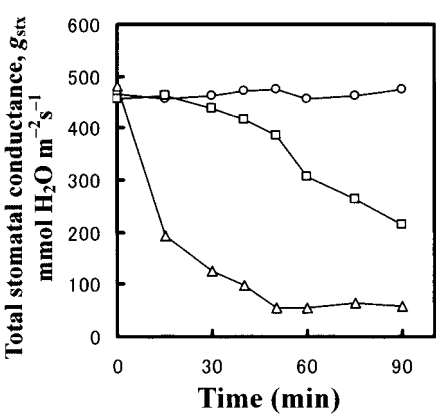

Fig. 3 Time courses of total stomatal conductance from 0 to 90 min after ABA treatment at each site indicated in Fig. 1. Symbols: circles (site 1), triangles (site 2), squares (site 3).

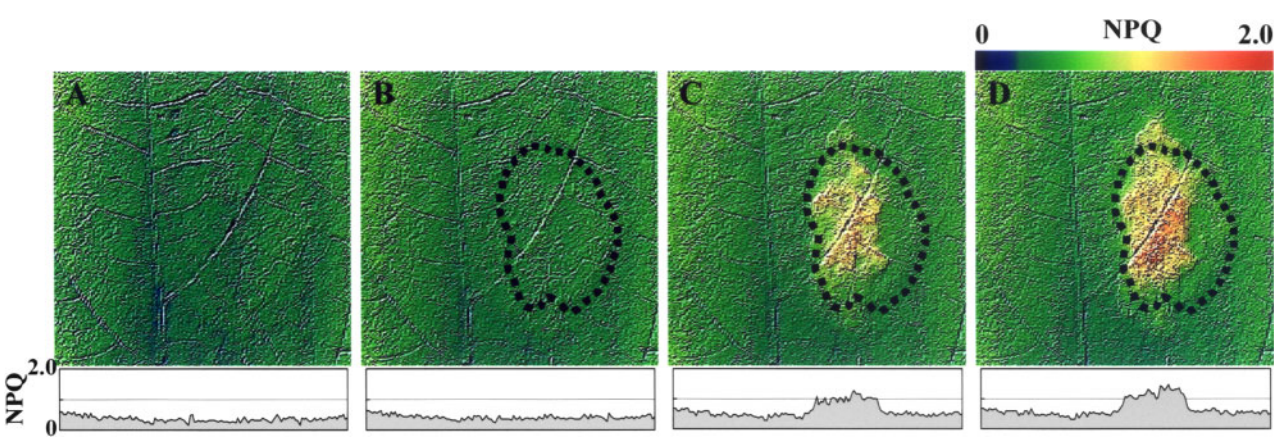

Fig. 4 Changes in the distribution of NPQ (indicated by color) in the measurement area shown in Fig. 1 from 0 to 90 min after ABA treatment. The cross-sectional diagrams represent transects of NPQ values across the NPQ images along the line X–X′ shown in Fig. 1. The region within the dotted line (B–D) is the ABA-treated region. Experimental conditions were as in Fig. 2. (A) Just before ABA treatment, and (B) 15 min, (C) 50 min, and (D) 90 min after ABA treatment.

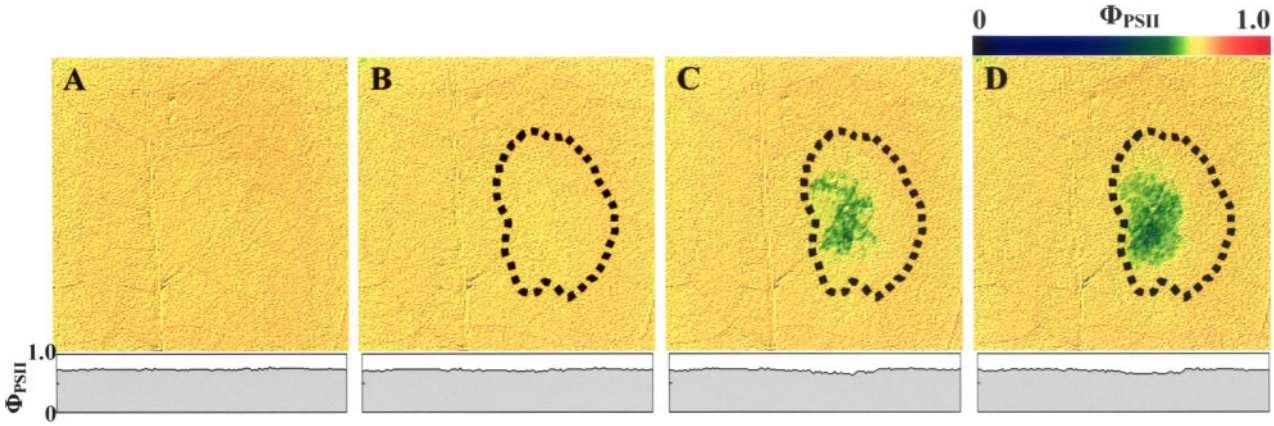

Fig. 5 Changes in the distribution of Φ_{PSII} (indicated by color) in the measurement area shown in Fig. 1 from 0 to 90 min after ABA treatment. The cross-sectional diagrams represent transects of Φ_{PSII} values across the Φ_{PSII} images along the line X–X′ shown in Fig. 1. The region within the dotted line (B–D) is the ABA-treated region. Experimental conditions were as in Fig. 2. (A) Just before ABA treatment, and (B) 15 min, (C) 50 min, and (D) 90 min after ABA treatment.

215 mmol m^{-2} s^{-1} at 90 min (Fig. 3). The stomatal conductance at an interveinal mesophyll site (site 1 in Fig. 1) separated by the midvein from the ABA-treated region showed no change and stayed between 457 and 475 mmol m^{-2} s^{-1} throughout the experiment (Fig. 3).

Fig. 4 and 5 show changes in the distributions of NPQ and Φ_{PSII} in the same leaf area as in Fig. 1 and 2 from 0 to 90 min after the ABA treatment. The NPQ and Φ_{PSII} values along line X–X′ (shown in Fig. 1) are represented below each image. Before ABA treatment, the NPQ and Φ_{PSII} values were uniformly distributed across the leaf area, with values in the ranges of 0.16 to 0.62 for NPQ and 0.72 to 0.77 for Φ_{PSII} except at the veins. Until 30 min after the ABA treatment, no change in NPQ or Φ_{PSII} was seen in the images or the time courses (Fig. 4–6). Thereafter, NPQ began to increase at the sites of severe stomatal closure and continued to increase with time (Fig. 6A). The most affected area were the same in Fig. 2 and 4. The NPQ value at site 2 reached 1.19 at 50 min and 1.50 at 90 min after the treatment (Fig. 6A). Increased NPQ values were limited to the areas showing severe stomatal closure, and

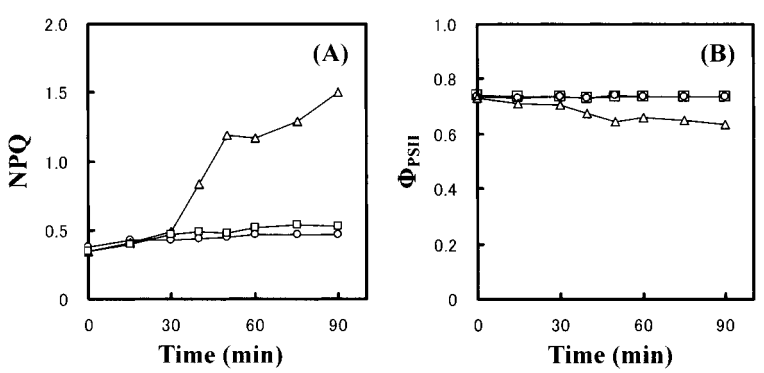

Fig. 6 Time courses of NPQ (A) and Φ_{PSII} (B) values from 0 to 90 min after ABA treatment at each site indicated in Fig. 1. Symbols: circles (site 1), triangles (site 2), squares (site 3).

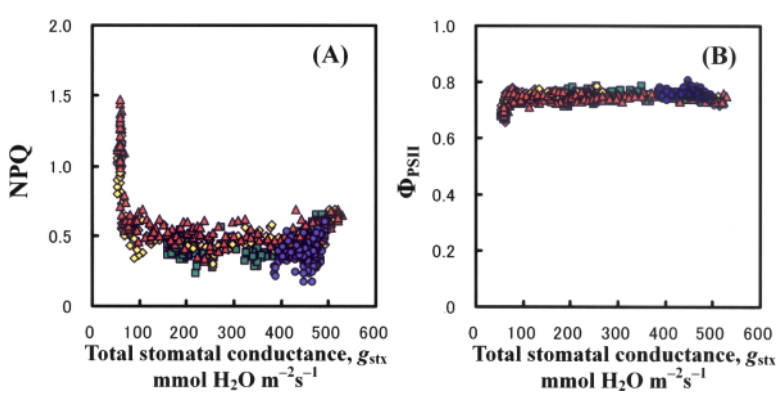

Fig. 7 Relationships between total stomatal conductance and fluorescence parameters, NPQ (A) and Φ_{PSII} (B), from 0 to 90 min after ABA treatment. Symbols: blue circles, green squares, yellow diamonds, and red triangles represent 0, 15, 50, and 90 min after ABA treatment, respectively. The 120 points plotted for each measurement time were taken along the line X–X′ shown in Fig. 1.

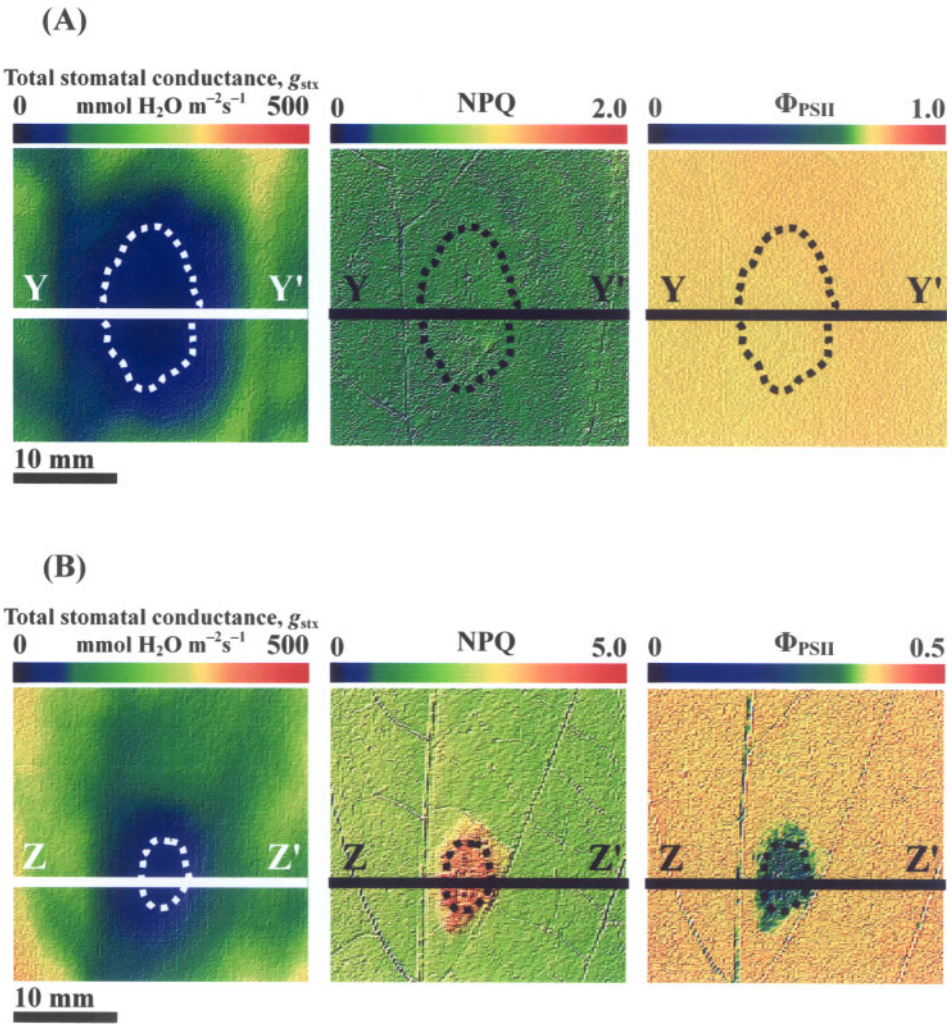

Fig. 8 Effects of ABA treatment on the distribution of total stomatal conductance, NPQ, and Φ_{PSII} on *P. vulgaris* L. leaves 90 min after ABA treatment under illumination at PPFs of 270 (A) and 700 (B) µmol m^{-2} s^{-1}. Other experimental conditions were as follows for PPFs of 270 and 700 µmol m^{-2} s^{-1}, respectively: air temperature, 26.5 and 25.3°C; relative humidity, 45% and 53%; short-wavelength radiation, 34.3 and 88.9 W m^{-2}; long-wavelength radiation, 0.98 and 1.16 kW m^{-2}; and boundary layer conductance for heat transfer, 14.5 and 34.4 mm s^{-1}.

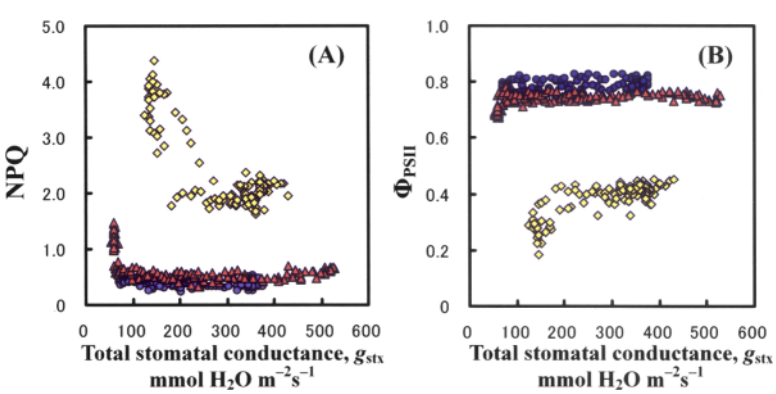

Fig. 9 Relationships between total stomatal conductance and fluorescence parameters, NPQ (A) and Φ_{PSII} (B), 90 min after ABA treatment under illumination at PPFs of 270 (blue circles), 350 (red triangles), and 700 (yellow diamonds) µmol m^{-2} s^{-1}. These data were obtained at sites along the lines X–X′, Y–Y′, Z–Z′ shown in Fig. 1 and 8 and correspond to the data shown in Fig. 2D, 4D, 5D, 8A, and 8B.

slight patchiness is also evident in these areas (Fig. 4C, D). The NPQ at sites 1 and 3 showed little change with time and remained in a range of 0.35 to 0.53 for 90 min, with a slight increasing trend; however, the increase was very small compared with the increase at site 2 induced by ABA treatment (Fig. 6A). Φ_{PSII} slightly decreased, but only in the areas that showed the most severe stomatal closure; the decrease at site 2 became evident only after 30 min, reaching 0.67 at 50 min after treatment (Fig. 6B). Afterwards, Φ_{PSII} stayed in the range of 0.65 to 0.68. Slight patchiness was observed in those sites (Fig. 5C, D). Φ_{PSII} at sites 1 and 3 showed no detectable change and remained in the range of 0.73 to 0.74 for 90 min (Fig. 6B).

Fig. 7 shows relationships between the total stomatal conductance and NPQ and Φ_{PSII} at sites along the line X–X′ shown in Fig. 1. NPQ stayed in the range of 0.16 to 0.69 when the total stomatal conductance was greater than 80 mmol m^{-2} s^{-1};

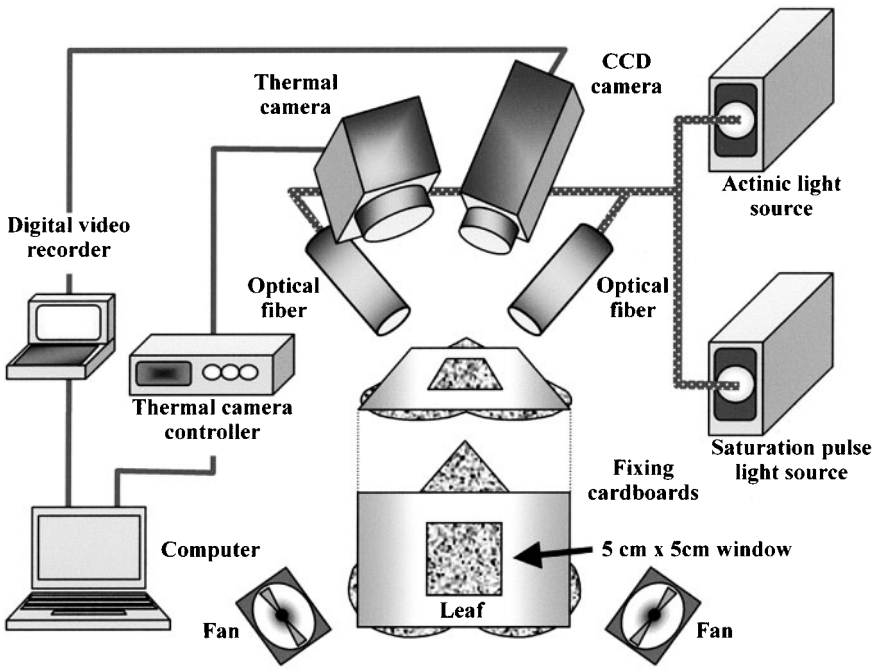

Fig. 10 Schematic diagram of the thermal and chlorophyll fluorescence imaging system. Image measurements were performed in an environmentally controlled measuring chamber. Environmental conditions (air temperature, relative humidity, short-wavelength radiation, long-wavelength radiation, and air current around the leaf surfaces) were kept uniform and constant during the experiment. An attached leaf was placed in an opaque cardboard frame (15×20 cm) with a 5×5 cm window and set horizontally in the measuring chamber.

however, it drastically increased as the total stomatal conductance values fell below 80 mmol m^{-2} s^{-1}. Before ABA treatment, most of the low-NPQ points (blue closed circle in Fig. 7A) with total stomatal conductance values greater than 450 mmol m^{-2} s^{-1} were located in mesophyll areas. The low-NPQ points moved towards the left and became the upper points with time after ABA treatment. Meanwhile, changes in Φ_{PSII} in relation to total stomatal conductance were very small; however, the pattern was somewhat similar to that of NPQ. The Φ_{PSII} values stayed in the range 0.69 to 0.77 when the total stomatal conductance was greater than 80 mmol m^{-2} s^{-1} and decreased somewhat when the total stomatal conductance was less than 80 mmol m^{-2} s^{-1}.

Fig. 8 shows the distributions of total stomatal conductance, NPQ, and Φ_{PSII} on *P. vulgaris* L. leaves 90 min after ABA treatment under illumination at PPFs of 270 (Fig. 8A) and 700 μmol m^{-2} s^{-1} (Fig. 8B). At the lower photon flux, the areas within and around the ABA-treated region showed a significant decrease in total stomatal conductance, which was 72 mmol m^{-2} s^{-1} at the center of the ABA-treated region. However, the NPQ and Φ_{PSII} values in these areas did not change. The values of total stomatal conductance, NPQ, and Φ_{PSII} in the areas not affected by the ABA treatment stayed in the ranges of 336 to 381 mmol m^{-2} s^{-1}, 0.26 to 0.47, and 0.76 to 0.82, respectively (Fig. 8A). At the higher photon flux, the areas within and around the ABA-treated region showed a decrease in total stomatal conductance, a strong increase in NPQ, and a marked decrease in Φ_{PSII}. At the center of the ABA-treated region, the total stomatal conductance, NPQ, and Φ_{PSII} were 125 mmol m^{-2} s^{-1}, 4.37, and 0.18, respectively (Fig. 8B). The values of total stomatal conductance, NPQ, and Φ_{PSII} in the areas not affected by the ABA treatment were in the ranges 370 to 430 mmol m^{-2} s^{-1}, 1.67 to 2.31, and 0.37 to 0.45, respectively (Fig. 8B).

Fig. 9 shows relationships between the total stomatal conductance and NPQ and Φ_{PSII} 90 min after ABA treatment under illumination at PPFs of 270 (blue closed circle), 350 (red closed triangle), and 700 (yellow diamond) μmol m^{-2} s^{-1}. At the lowest photon flux, NPQ and Φ_{PSII} did not change, regardless of the decrease in the total stomatal conductance. At the intermediate level of photon flux, the fluorescence parameters remained constant at total stomatal conductance values greater than 80 mmol m^{-2} s^{-1}, but they changed drastically below 80 mmol m^{-2} s^{-1}, as mentioned above (see Fig. 7). At the highest photon flux, the NPQ and Φ_{PSII} values stayed in the ranges 1.67 to 2.67 and 0.33 to 0.45, respectively, at total stomatal conductance values greater than 200 mmol m^{-2} s^{-1}. However, the fluorescence parameters changed drastically when the total stomatal conductance decreased to less than about 200 mmol m^{-2} s^{-1}. The general patterns of the relationships between the total stomatal conductance and the fluorescence parameters were similar to those observed at the intermediate PPF, even though the absolute values were very different.

Discussion

A new imaging system capable of concurrent, quantitative, straightforward evaluation of stomatal conductance, NPQ, and Φ_{PSII} of intact attached leaves solely under aerobic conditions, using both thermal imaging and chlorophyll fluorescence imaging was developed. Using this system, we investigated relationships between the spatiotemporal variations of stomatal conductance and of NPQ and Φ_{PSII} across intact *P. vulgaris* L.

leaves in response to ABA treatment at each 0.1×0.1 mm site under three actinic light intensities.

Stomatal conductance is an indicator of the extent of stomatal opening: it decreases when the stomata close and vice versa (Omasa et al. 1983, Jones 1992). Spatiotemporal variations in the total stomatal conductance were evaluated from leaf temperature images measured by thermal imaging under constant thermal conditions. In experiments performed at PPFs of 270, 350, and 700 μmol m^{-2} s^{-1}, the distributions of total stomatal conductance in the mesophyll areas before ABA treatment were constant (e.g. Fig. 2A). The mean value of the total stomatal conductance ranged from 330 to 512 mmol m^{-2} s^{-1}, which indicates that the stomata were well opened (Omasa et al. 1983, Omasa and Croxdale 1992, Jones 1999). In an experiment under illumination at a PPF of 350 μmol m^{-2} s^{-1}, the total stomatal conductance in the ABA-treated region rapidly decreased in the first 15 min after the ABA treatment (Fig. 2B). In particular, the center of the ABA-treated region (Fig. 3) showed a substantial decrease in total stomatal conductance (approximately an 80% decrease) compared with the rest of the ABA-treated region. The total stomatal conductance continued to decrease to less than 60 mmol m^{-2} s^{-1} by 50 min after the ABA treatment (Fig. 2C, 3). Thereafter, it stopped and stayed at the minimum value of 60 mmol m^{-2} s^{-1} until 90 min after the ABA treatment (Fig. 2D, 3). These results show that ABA induced rapid stomatal closure and diminished the total stomatal conductance to a minimum value in less than an hour. The minimum value of the total stomatal conductance did not reach zero, however. One reason may be that the ABA treatment could not induce complete stomatal closure. Another may be that cuticular transpiration was not negligible when the stomatal apertures were severely closed (Meyer and Genty 1998). Or third, the calculation of stomatal conductance from leaf temperature may have had an error (Omasa et al. 1981a, Omasa and Croxdale 1992).

Spatiotemporal variations in the total stomatal conductance revealed the diffusion of ABA in the leaf tissue (Fig. 2). Although the area of low total stomatal conductance expanded in almost all directions from 15 to 50 min after the ABA treatment (Fig. 2B, C), the rate at which the area with low total stomatal conductance expanded toward the leaf margin along a lateral vein was faster than in other directions between 50 and 90 min after ABA treatment (Fig. 2C, D). These results show that the initial expansion of the area with low total stomatal conductance depended on ABA diffusion, induced by the ABA concentration gradient through apoplasts and veinlets, and the subsequent expansion toward the leaf edge depended mainly on ABA transportation by the transpiration stream in the vein, in addition to the former mechanism of expansion. This interpretation is confirmed by the time course of changes in total stomatal conductance at a site 6–7 mm away from the ABA-treated region, closer to the leaf margin along a lateral vein (site 3 in Fig. 1 and 3). The initial rate of expansion was approximately 11.4 mm h^{-1}, and this rate was maintained along the lateral vein (Fig. 2D). On the other hand, total stomatal conductance at a mesophyll site separated by the midvein from the ABA-treated region remained at the initial values throughout the experiment, indicating that ABA did not cross the midvein (see site 1 in Fig. 1–3).

At PPFs of 270 and 700 μmol m^{-2} s^{-1}, the values of total stomatal conductance at the sites not affected by ABA treatment were relatively lower than at a PPF of 350 μmol m^{-2} s^{-1} (Fig. 2D, 8, 9). This may be attributed to differences in the individual leaves used for the experiments and in the environmental conditions, including the light intensities. At 90 min after ABA treatment, the minimum value, approximately 125 mmol m^{-2} s^{-1}, of total stomatal conductance occurred at a PPF of 700 μmol m^{-2} s^{-1}; this value was higher than those obtained at PPFs of 270 and 350 μmol m^{-2} s^{-1} (Fig. 9). This may have been due to differences in the amount of ABA solution absorbed by the leaves.

Chlorophyll fluorescence imaging reveals the effects of ABA treatment on non-photochemical quenching and on the yield of linear electron transport through PSII. At a PPF of 350 μmol m^{-2} s^{-1}, NPQ and Φ_{PSII} values were uniformly distributed over the leaf surface before ABA treatment (Fig. 4A, 5A). The mean value of NPQ was low and that of Φ_{PSII} was high, because the experiment was performed under aerobic conditions (Bro et al. 1996, Meyer and Genty 1998, Meyer and Genty 1999). But 15 min and even 90 min after ABA treatment, mesophyll areas with total stomatal conductance values greater than about 80 mmol m^{-2} s^{-1} and without any change in NPQ or Φ_{PSII} were observed (Fig. 2, 4, 5). This shows that ABA treatment induced only stomatal closure, without affecting the non-photochemical quenching or the yield of linear electron transport through PSII in these mesophyll areas (Fig. 7). The lack of changes in Φ_{PSII} suggested that photorespiration was active and consumed any excess light energy in those areas, thus protecting the photosynthetic apparatus from photoinhibitory damage (Osmond 1981, Sharkey et al. 1988, Cornic and Briantais 1991, Brestic et al. 1995, Ort 2001, Ort and Baker 2002). Consequently, the NPQ in those areas did not change, because an extreme intrathylakoid pH gradient was not generated, owing to cooperative consumption of light energy by CO_2 fixation and photorespiration (Müller et al. 2001). This phenomenon was also observed at a PPF of 270 μmol m^{-2} s^{-1}, even though the total stomatal conductance reached a minimum value of approximately 70 mmol m^{-2} s^{-1} (blue closed circles in Fig. 9). Moreover, a similar phenomenon occurred at a PPF of 700 μmol m^{-2} s^{-1} when the total stomatal conductance was over 200 mmol m^{-2} s^{-1} (yellow closed diamonds in Fig. 9).

In contrast, in the experiment at a PPF of 350 μmol m^{-2} s^{-1}, when stomatal apertures were severely closed and the total stomatal conductance was extremely decreased to less than 80 mmol m^{-2} s^{-1} at 50 min after ABA treatment, Φ_{PSII} began to decrease slightly at the center of the ABA-treated region (Fig. 2C, 5C, 6B, 7B). Simultaneously, NPQ began to increase in those areas (Fig. 2C, 4C, 6A, 7A). This suggests that, when the

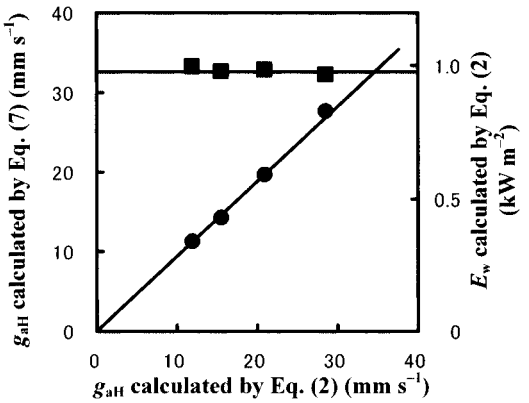

Fig. 11 A comparison of g_{aH} calculated from Eq. (2) and g_{aH} calculated from Eq. (7) under several air current conditions at a PPF of 350 μmol m^{-2} s^{-1}. Long-wavelength radiation from the environment (E_w) was evaluated by substituting g_{aH} in Eq. (2). The absorption coefficient of the short-wavelength radiation of the black felt model leaf was 0.98±0.02. The long-wavelength emissivity of the model leaf was 0.98±0.02. The experimental conditions were as follows: short-wavelength radiation, 44.5 W m^{-2}; air temperature, 26.5±0.1°C; and relative humidity, 48%.

stomatal apertures were severely closed and the CO_2 supply through the stomata was severely inhibited, the linear electron transport chain became over-reduced, and cyclic electron transport around PSI and electron transport to the water–water cycle were activated (Schreiber and Neubauer 1990, Asada 1999, Ort 2001, Ort and Baker 2002). These alternative electron transport systems generate a large intrathylakoid pH gradient and activate dissipation of the excess light energy as heat by means of the xanthophyll cycle (Müller et al. 2001, Ort 2001, Ort and Baker 2002). Our results showed that, when a slight decrease in the yield of linear electron transport through PSII (Φ_{PSII}) was observed, heat dissipation of the excess light energy was activated, to protect the photosynthetic apparatus from photoinhibitory damage. This phenomenon was also observed at a PPF of 700 μmol m^{-2} s^{-1} when the total stomatal conductance decreased to less than 200 mmol m^{-2} s^{-1} (yellow closed diamonds in Fig. 9). However, this phenomenon was not apparent in the experiment under illumination at a PPF of 270 μmol m^{-2} s^{-1} (blue closed circles in Fig. 9), because the light intensity was too weak to activate the heat-dissipation process.

We interpret the relationships between the total stomatal conductance and the fluorescence parameters at the various actinic light intensities as follows. If the actinic light intensity is weak enough (e.g. PPF = 270 μmol m^{-2} s^{-1} in our experiment), the fluorescence parameters do not change even though the total stomatal conductance reaches its minimum value. If the actinic light intensity is strong enough (e.g. PPF = 350 or 700 μmol m^{-2} s^{-1} in our experiment), the fluorescence parameters change drastically when the total stomatal conductance decreases to less than a specific value. The specific value is higher at higher actinic light intensities (e.g. 80 mmol m^{-2} s^{-1} for 350 μmol m^{-2} s^{-1} and 200 mmol m^{-2} s^{-1} for 700 μmol m^{-2} s^{-1}). Such specific values cannot be detected by conventional point data measurements, because the conventional point data measurements measure average values of a selected leaf area that shows heterogeneous responses to environmental stimuli (Omasa 1990, Omasa and Croxdale 1992, Terashima 1992, Beyschlag and Eckstein 1998). For example, it has been reported that the heat-dissipation process is gradually activated with respect to decreasing stomatal conductance during water stress (Flexas et al. 2002). However, in our experiment, image analysis of the relationship between stomatal conductance and chlorophyll fluorescence parameters at a resolution of 0.1 mm revealed that the heat-dissipation process is rapidly activated only when the absorbed light energy exceeds energy consumption by CO_2 fixation and photorespiration within each mesophyll site. Our study has, for the first time, quantitatively analyzed relationships between spatiotemporal variations in total stomatal conductance and chlorophyll fluorescence parameters on a 0.1×0.1 mm grid of intact leaves under exclusively aerobic conditions, by using both thermal imaging and chlorophyll fluorescence imaging.

Materials and Methods

Plant material

Kidney bean (*P. vulgaris* L. cv. 'Shin-edogawa') seeds were sown in pots (12 cm in diameter and 10 cm tall) in an environmentally controlled growth chamber, and the plants were grown for 4 weeks. The pots were filled with artificial soil (mixture of vermiculite and perlite, 1 : 1, v/v). The plants were illuminated for 12 h each day with fluorescent lights at a PPF of 300 μmol m^{-2} s^{-1}. Air temperature was 26.5°C during the day and 20.0°C at night. Relative humidity was 45% during the day and 60% at night. Plants were watered daily with a nutrient solution (1 : 1,000 dilution of HYPONeX). Fully expanded mature leaves were used in situ for the experiments. The ratio of the stomatal frequency on the upper surface to that on the lower surface was about 1 : 8.2. The leaves were 0.08 to 0.15 mm thick. The difference in leaf temperature between upper and lower surfaces was about 0.1°C at a PPF of 350 μmol m^{-2} s^{-1}.

Computer-aided imaging system for combining thermal imaging and chlorophyll fluorescence imaging

Fig. 10 shows a scheme of the computer-aided imaging system for combining thermal imaging and chlorophyll fluorescence imaging. Thermal images, for calculating stomatal conductance, were measured with an optical-mechanical scanning thermographic system (JEOL, JTG-5200, thermal camera and controller) with an HgCdTe detector (8–13 μm, cooled by liquid nitrogen) having a temperature resolution of 0.05°C. The detected signals were converted into 16-bit resolution digital signals (512 horizontal × 480 vertical pixels) and recorded as digital data to a hard disk in the thermal camera controller. After the data were transferred to the computer, they were converted to exact-temperature images by using an equation determined by comparing the temperatures of dry and wet model leaves with black felt surfaces on both sides (the absorption coefficient of short-wavelength radiation was 0.98 and the emissivity of long-wavelength radiation was 0.98 in the model leaf) as measured with the thermographic system and with thermocouples (Omasa et al. 1981a, Omasa and Croxdale 1992). The distance from the thermal camera to the leaf surface was 0.35 m, and the spatial resolution of the thermal image was about 0.1 mm. By measuring the thermal image of leaf having a drastic change in the

temperature distribution, we confirmed that the effect of heat conduction on the spatial distribution of leaf temperature was small.

Chlorophyll fluorescence images were measured with a cooled charge-coupled device (CCD) video camera (Hamamatsu Photonics, C5985-02) equipped with an interference filter (Optical Coatings Japan, IF-W, λ = 683 nm, half-band width = 10 nm) and a long-pass filter (Corning, 2–64; λ >640 nm). The images were recorded on a digital video recorder (Sony, DSR-V10) at 640 horizontal × 480 vertical pixels per frame with 8-bit resolution and were analyzed by self-produced software. Continuous actinic light (PPF values of 270, 350, and 700 μmol m^{-2} s^{-1}) for photosynthesis was provided by a 150-W halogen lamp (Nikon, PSM-11520) equipped with a short-pass filter (Corning, 4–96; λ <620 nm) and was passed through two heat-absorbnsing filters via an optical fiber system. A saturation light pulse (PPF 2,800 μmol m^{-2} s^{-1} for 1 s), to cause a transient saturation of photochemistry, was provided by two 180-W metal halide lamps (Sumita Optical Glass, Inc., LS-M180) and passed through a short-pass filter (Corning, 4–96; λ <620 nm) and a heat-absorbing filter via an optical fiber system.

An in-situ leaf (i.e. a leaf that remained attached to the plant) was sandwiched between two opaque pieces of cardboard (15×20 cm) having a 5×5 cm window in the same place. The sandwich was mounted horizontally in the measuring chamber containing an atmosphere of approximately 21% O_2 and 560 ppm CO_2 (Fig. 10). The spatial distributions of the boundary-layer conductance of the upper and lower surfaces of the leaf within the window were kept constant by controlling the air current with small electric fans. The actinic light intensity and other environmental conditions such as air temperature, relative humidity, short-wavelength radiation, and long-wavelength radiation were also kept constant over the leaf area in the window. Thermal imaging and chlorophyll fluorescence imaging were performed simultaneously after the leaf's photosynthesis reached steady state. The measured images were analyzed by both self-produced software and commercial software (ERDAS, ERDAS IMAGINE Ver. 8.3). Geometrical deformation of images was corrected by affine transformation within an error of 1 pixel at each position regardless of image type.

Calculation of total stomatal conductance image from leaf temperature image

Spatial distributions of stomatal conductance to water vapor diffusion across a leaf surface can be quantitatively evaluated from the leaf temperature image as measured by a thermographic system (Omasa et al. 1981a, Omasa and Croxdale 1992). In this study, the total stomatal conductance was computed as the sum of the values on both sides of the leaf, although the stomatal conductance of the upper surface differed from that of the lower surface (Omasa et al. 1983, Jones 1992).

Water evaporates from mesophyll and epidermal cell walls and diffuses into the air through the stomata and boundary layer. If the leaf temperature and boundary layer are assumed to be equal on both sides, the transpiration rate, W_x (g mm^{-2} s^{-1}), at each leaf site is expressed by

$$W_x = \frac{X(T_{lx}) - hX(T_a)}{1/g_{sux} + 1/g_{aWx}} + \frac{X(T_{lx}) - hX(T_a)}{1/g_{slx} + 1/g_{aWx}} \quad (1)$$

where T_{lx} is the leaf temperature (°C), T_a is the air temperature (°C), $X(T)$ is the saturated water vapor density at T °C (g mm^{-3}), h is the relative humidity of the air, g_{sux} is the stomatal conductance to water vapor diffusion of the upper leaf surface (mm s^{-1}), g_{slx} is the stomatal conductance to water vapor diffusion of the lower leaf surface (mm s^{-1}), and g_{aWx} is the boundary layer conductance to water vapor diffusion (mm s^{-1}). The subscript x denotes the values at the local site (x) on the leaf. Because the difference in leaf temperature between the upper and lower surfaces was about 0.1°C, this assumption was reasonable.

Considering the heat balance at each leaf site x, the transpiration rate at the leaf site can be described by the following simplified equation:

$$W_x = \frac{1}{L} \times [\alpha_p E_{sx} + \varepsilon\{E_{wx} - 2\sigma(273.15 + T_{lx})^4\} + 2g_{aHx}\rho c_p(T_a - T_{lx})] \quad (2)$$

where E_{sx} is the short-wavelength radiation from the environment (W m^{-2} at wavelengths ≤3 μm), E_{wx} is the long-wavelength radiation from the environment (W m^{-2} at wavelengths ≥3 μm), α_p is the absorption coefficient of short-wavelength radiation of the leaf, ε is the emissivity of long-wavelength radiation of the leaf, σ is the Stefan–Boltzmann constant (5.67×10^{-8} W m^{-2} K^{-4}), g_{aHx} is the boundary layer conductance to heat transfer (mm s^{-1}), ρc_p is the volumetric heat capacity of air (1.192 kW s m^{-3} $°C^{-1}$), and L is the latent heat of evaporation (2.44 kW s g^{-1}). When the environmental conditions such as air temperature, relative humidity, radiation (long-wavelength and short-wavelength), and air current (boundary layer conductance) around the leaf surface are kept constant at the leaf site, only the leaf temperature, T_{lx}, remains as a variable on the right side of Eq. (2). Therefore, the transpiration rate at the leaf site can be evaluated from the measured leaf temperature (T_{lx}).

Meanwhile, g_{aWx} used in Eq. (1) can be expressed with g_{aHx} used in Eq. (2):

$$g_{aWx} = (D_W / D_H)^{2/3} g_{aHx} \quad (3)$$

where D_H is the thermal diffusivity in air (22.3 mm^2 s^{-1}), and D_W is the water vapor diffusivity in air (25.1 mm^2 s^{-1}) (Jones 1992). Consequently, the total stomatal conductance to water vapor diffusion at each leaf site can be evaluated from Eqs. (1), (2), and (3) when the parameters other than T_{lx} are known. To be specific, W_x is first calculated by Eq. (2) from the leaf temperature (T_{lx}). Second, W_x in Eq. (1) is substituted for the value of W_x determined from Eq. (2). At the same time, g_{aWx} in Eq. (1) is substituted for $g_{aHx}/(D_H/D_W)^{2/3}$ determined from Eq. (3), and g_{sux} in Eq. (1) is substituted for g_{slx} multiplied by the ratio of the number of stomata on the upper surface to those on the lower surface. Finally, g_{slx} in Eq. (1) is determined by solving the quadratic equation; subsequently, the total stomatal conductance to water vapor diffusion (g_{stx}) is computed as the sum of the values from each side (heat balance method):

$$g_{stx} = g_{sux} + g_{slx} = \left(\frac{R_{st} + 1}{R_{st}}\right) g_{slx} \quad (4)$$

where R_{st} is the ratio of the number of stomata on the lower leaf surface to those on the upper leaf surface. The units of total stomatal conductance to water vapor diffusion were converted into molar units (mmol m^{-2} s^{-1}) from mass units (mm s^{-1}) (40 mmol m^{-2} s^{-1} = 1 mm s^{-1}; Jones 1999).

Calculation of NPQ and Φ_{PSII} images from a set of fluorescence intensity images

A set of fluorescence intensity images (^iF, $^iF_m'$, and ^iF_m) was used for the calculation of the NPQ and Φ_{PSII} images. After stomatal opening reached steady state under a given light flux, an image ^iF was measured. Just after the measurement, an $^iF_m'$ image was measured during a saturation light pulse during steady-state photosynthesis. Finally, an ^iF_m image was measured during a saturation light pulse after the leaf was held in darkness for at least 1 h after the experiments. Each fluorescence intensity image (^iF, $^iF_m'$, and ^iF_m) was divided by the average value of fluorescence emitted from a fluorescent standard induced by the corresponding light intensity to convert it into a relative fluorescence yield image.

Using the relative fluorescence yield images, images (640 horizontal × 480 vertical pixels, 8-bit resolution) of NPQ and Φ_{PSII} were made by computing each pixel with the following equations (Genty et al. 1989, Bilger and Björkman 1990, Maxwell and Johnson 2000):

$$NPQ = \frac{{}^{i}F_m/R_{SL} - {}^{i}F_m'/R_{SL}}{{}^{i}F_m'/R_{SL}} = \frac{{}^{i}F_m - {}^{i}F_m'}{{}^{i}F_m'} \quad (5)$$

and

$$\Phi_{PSII} = \frac{{}^{i}F_m'/R_{SL} - {}^{i}F/R_{AL}}{{}^{i}F_m'/R_{SL}} \quad (6)$$

where R_{SL} and R_{AL} are the average values of fluorescence emitted from the fluorescent standard induced by the saturation light pulse and the actinic light, respectively.

The NPQ image, with pixel values ranging from zero to infinity, represents the extent of the intrathylakoid pH gradient and the ability of chloroplasts to dissipate excess excitation energy as heat (Bilger and Björkman 1990, Maxwell and Johnson 2000). The Φ_{PSII} image represents the yield of linear electron transport through PSII, with pixel values ranging from 0 to 1 (Genty et al. 1989, Maxwell and Johnson 2000).

Measurement of thermal environments and parameters

To calculate the total stomatal conductance by the above-mentioned heat-balance method, the thermal environment and the parameters in Eq. (1) and Eq. (2) have to be known. The air temperature (T_a) and relative humidity (h) in the measuring chamber were kept at 26.5±0.1°C and 48% for PPFs of 270 and 350 μmol m^{-2} s^{-1} and at 25.3±0.1°C and 53% for the PPF of 700 μmol m^{-2} s^{-1}. Other thermal environmental conditions were kept constant around the leaf area in the window. Actinic light intensity (PPF) and short-wavelength radiation (E_{sx}) were 350 μmol m^{-2} s^{-1} and 44.5 W m^{-2}, 270 μmol m^{-2} s^{-1} and 34.3 W m^{-2}, and 700 μmol m^{-2} s^{-1} and 88.9 W m^{-2}; these parameters were measured with quantum and photosynthetically active radiation (PAR) sensors (LI-185A, LI-COR), because the wavelengths of the actinic light were almost all in the PAR range. The spatial distributions of PPF and E_{sx} were kept within ±5% of the mean value in the 5×5 cm window and within ±2.5% of the mean value in the 3×3 cm area in the center of the window by adjusting the optical fiber system. The long-wavelength radiation (E_{wx}) from the environment and the boundary layer conductance to heat transfer (g_{aHx}) were determined by solving simultaneous equations of Eq. (2) developed using dry and wet model leaves with black felt surfaces on both sides, where the absorption coefficient (α_p) of the short-wavelength radiation measured with the LI-185A sensor was 0.84 for a kidney bean leaf and 0.98 for the model leaf, and the emissivity (ε) of long-wavelength radiation measured by the thermographic system was 0.98 for both kidney bean and model leaves. Consequently, E_{wx} and g_{aHx} were determined to be 0.98 kW m^{-2} and 12.0 mm s^{-1} for the experiment at a PPF of 350 μmol m^{-2} s^{-1}, 0.98 kW m^{-2} and 14.5 mm s^{-1} for the experiment at a PPF of 270 μmol m^{-2} s^{-1}, and 1.16 kW m^{-2} and 34.4 mm s^{-1} for the experiment at a PPF of 700 μmol m^{-2} s^{-1}, respectively. The thermal environmental conditions in the measuring chamber determined the values of E_{wx}. The temperatures estimated from the values of E_{wx} at PPFs of 270, 350, and 700 μmol m^{-2} s^{-1} were 90°C, 90°C, and 105°C, respectively. The high temperatures seemed to be due to the light sources in the measurement chamber. Boundary layer conductance to heat transfer was kept constant at each site on both sides of the leaf area by adjusting the air current. The temperature distribution of the black felt model leaf was maintained within 0.1°C except for the edges of the window.

The value of g_{aH} can be determined by substituting Eq. (3) for Eq. (1) using a wet black felt model leaf. The W in Eq. (1) was obtained by measuring changes in weight of the wet model leaf, where g_{su} and g_{sl} in Eq. (1) were assumed to be infinity. Therefore, g_{aH} can be expressed with the following equation:

$$g_{aH} = \frac{W(D_H/D_W)^{2/3}}{2\{X(T_l) - hX(T_a)\}} \quad (7)$$

To assess the measurement error of the thermographic system, we obtained the g_{aH} by solving simultaneous equations of Eq. (2) with input parameters determined from measurements on dry and wet black felt model leaves (α_p was 0.98. ε was 0.98. g_{su} and g_{sl} were assumed to be infinity). This value was compared with g_{aH} determined by Eq. (7) (Fig. 11). The difference between g_{aH} obtained by solving simultaneous equations of Eq. (2) and that calculated by substituting W measured by the weighing method for Eq. (7) was within 8% regardless of g_{aH} values. The error in E_w obtained by the simultaneous equations of Eq. (2) was within 1.7% of the mean value.

Simultaneous measurement of spatiotemporal variations of stomatal conductance, NPQ, and Φ_{PSII} in response to ABA treatment

Using the above-described system, we investigated the effects of the ABA treatment on the total stomatal conductance, NPQ, and Φ_{PSII} of in situ *P. vulgaris* L. leaves under three intensities of actinic light. An attached leaf mounted in an opaque cardboard frame (Fig. 10) was horizontally placed in the measuring chamber after the controlled thermal environmental conditions were measured by using the black felt model leaf by the methods described above. The R_{st} in Eq. (4) for kidney bean leaves used in this experiment was 8.2. The leaf was adapted to the environmental conditions for 2 h, which allowed the stomatal opening and the photosynthetic activities to reach steady state. This was confirmed by low values, constancy, and uniform distribution of temperature and chlorophyll fluorescence intensity (^{i}F) over the leaf area as obtained by monitoring thermal and chlorophyll fluorescence images. Then, control images of leaf temperature and ^{i}F and $^{i}F_m'$ images of chlorophyll fluorescence were measured in sequence. The influence of the saturation light pulse used for $^{i}F_m'$ measurement (as a heat pulse) disappeared within about 20 s. Thus the saturation light pulse did not cause any changes in stomatal opening. Just after the control measurement, 10^{-3} M ABA (Wako, 97.0% purity) was applied to both leaf sides of a small mesophyll region (Fig. 1) with a brush. After the treatment, a temporary decrease in leaf temperature was observed in the treated region, because of evaporation of the ABA solution. This effect disappeared within 10 min with loss of the solution. Afterwards, images of leaf temperature, ^{i}F, and $^{i}F_m'$ were measured at intervals of 10 or 15 min, except for the initial 15 min, for 90 min after the ABA treatment. Finally, an $^{i}F_m$ image was measured after the leaf area was kept in darkness for at least 1 h. Images of total stomatal conductance, NPQ, and Φ_{PSII} were calculated from the images of leaf temperature and the set of chlorophyll fluorescence intensity images (^{i}F, $^{i}F_m'$, and $^{i}F_m$).

Acknowledgments

We thank Takateru M. Uenishi and Ryosuke Endo for helpful discussion and comments on the manuscript. We are grateful to the Japan Society for the Promotion of Science for funding this study.

References

Asada, K. (1999) The water–water cycle in chloroplasts: scavenging of active oxygens and dissipation of excess photons. *Annu. Rev. Plant Physiol. Plant Mol. Biol.* 50: 601–639.

Beyschlag, W. and Eckstein, J. (1998) Stomatal patchiness. *In* Progress in Botany, Vol. 59. Edited by Behnke, H.D., Esser, K., Kadereit, J.W., Lüttge, U. and Runge, M. pp. 283–298. Springer, Berlin.

Bilger, W. and Björkman, O. (1990) Role of the xanthophyll cycle in photoprotection elucidated by measurements of light-induced absorbance changes, fluorescence and photosynthesis in leaves of *Hedera canarienisis*. *Photosynth. Res.* 25: 173–185.

Brestic, M., Cornic, G., Fryer, M.J. and Baker, N.R. (1995) Does photorespiration protect the photosynthetic apparatus in French bean leaves from photoinhibition during drought stress? *Planta* 196: 450–457.

Bro, E., Meyer, S. and Genty, B. (1996) Heterogeneity of leaf CO_2 assimilation during photosynthetic induction. *Plant Cell Environ.* 19: 1349–1358.

Chaerle, L. and Straeten, D.V.D. (2000) Imaging techniques and the early detection of plant stress. *Trends Plant Sci.* 5: 495–501.

Cornic, G. and Briantais, J.M. (1991) Partitioning of photosynthetic electron flow between CO_2 and O_2 reduction in a C_3 leaf (*Phaseolus vulgaris* L.) at different CO_2 concentrations and during drought stress. *Planta* 183: 178–184.

Croxdale, J.G. and Omasa, K. (1990) Chlorophyll *a* fluorescence and carbon assimilation in developing leaves of light-grown cucumber. *Plant Physiol.* 93: 1078–1082.

Daley, P.F. (1995) Chlorophyll fluorescence analysis and imaging in plant stress and disease. *Can. J. Plant Pathol.* 17: 167–173.

Daley, P.F., Raschke, K., Ball, J.T. and Berry, J.A. (1989) Topography of photosynthetic activity of leaves obtained from video images of chlorophyll fluorescence. *Plant Physiol.* 90: 1233–1238.

Eckstein, J., Beyschlag, W., Mott, K.A. and Ryel, R.J. (1996) Changes in photon flux can induce stomatal patchiness. *Plant Cell Environ.* 19: 1066–1074.

Ellenson, J.L. and Amundson, R.G. (1982) Delayed light imaging for the early detection of plant stress. *Science* 215: 1104–1106.

Flexas, J., Escalona, J.M., Evain, S., Gulías, J., Moya, I., Osmond, C.B. and Medrano, H. (2002) Steady-state chlorophyll fluorescence (Fs) measurements as a tool to follow variations of net CO_2 assimilation and stomatal conductance during water stress in C_3 plants. *Physiol. Plant.* 114: 231–240.

Genty, B., Briantais, J.M. and Baker, N.R. (1989) The relationship between the quantum yield of photosynthetic electron transport and quenching of chlorophyll fluorescence. *Biochim. Biophys. Acta* 990: 87–92.

Genty, B. and Meyer, S. (1995) Quantitative mapping of leaf photosynthesis using chlorophyll fluorescence imaging. *Aust. J. Plant Physiol.* 22: 277–284.

Govindjee (1995) Sixty-three years since Kautsky: Chlorophyll a fluorescence. *Aust. J. Plant Physiol.* 22: 131–160.

Govindjee and Nedbal, L. (2000) The chlorophyll fluorescence imaging and its application in plant science and technology. Seeing is believing. *Photosynthetica* 38: 481–482.

Häder, D.P. (2000) *Image Analysis: Methods and Applications*. p. 463. CRC Press, Boca Raton.

Hashimoto, Y., Ino, T., Kramer, P.J., Naylor, A.W. and Strain, B.R. (1984) Dynamic analysis of water stress of sunflower leaves by means of a thermal image processing system. *Plant Physiol.* 76: 266–269.

Hashimoto, Y., Kramer, P.J., Nonami, H. and Strain, B.R. (1990) *Measurement Techniques in Plant Science.* pp. 343–431. Academic Press, San Diego.

Horler, D.N.H., Barber, J. and Barringer, A.R. (1980) Effects of cadmium and copper treatments and water stress on the thermal emission from peas (*Pisium sativum* L.): controlled environment experiments. *Remote Sens. Environ.* 10: 191–199.

Inoue, Y., Kimball, B.A., Jackson, R.D., Pinter, P.J. Jr. and Reginato, R.J. (1990) Remote estimation of leaf transpiration rate and stomatal resistance based on infrared thermometry. *Agr. Forest Meteorol.* 51: 21–33.

Jones, H.G. (1992) *Plants and microclimate*, *Edn. 2*. p. 428. Cambridge University Press, Cambridge.

Jones, H.G. (1999) Use of thermography for quantitative studies of spatial and temporal variation of stomatal conductance over leaf surfaces. *Plant Cell Environ.* 22: 1043–1055.

Kramer, P.J. and Boyer, J.S. (1995) *Water Relations of Plants and Soils*. pp. 162–164, 244–245. Academic Press, San Diego.

Krause, G.H. and Weis, E. (1991) Chlorophyll fluorescence and photosynthesis: the basics. *Annu. Rev. Plant Physiol. Plant Mol. Biol.* 42: 313–349.

Lichtenthaler, H.K., Lang, M., Sowinska, M., Heisel, F. and Miehé, J.A. (1996) Detection of vegetation stress via a new high resolution fluorescence imaging system. *J. Plant Physiol.* 148: 599–644.

Lichtenthaler, H.K. and Miehé, J.A. (1997) Fluorescence imaging as a diagnostic tool for plant stress. *Trends Plant Sci.* 2: 316–320.

Maxwell, K. and Johnson, G.N. (2000) Chlorophyll fluorescence: a practical guide. *J. Exp. Bot.* 51: 659–668.

Meyer, S. and Genty, B. (1998) Mapping intercellular CO_2 mole fraction (C_i) in *Rosa rubiginosa* leaves fed with abscisic acid by using chlorophyll fluorescence imaging: significance of C_i estimated from leaf gas exchange. *Plant Physiol.* 116: 947–957.

Meyer, S. and Genty, B. (1999) Heterogeneous inhibition of photosynthesis over the leaf surface of *Rosa rubiginosa* L. during water stress and abscisic acid treatment: induction of a metabolic component by limitation of CO_2 diffusion. *Planta* 210: 126–131.

Mott, K.A. (1995) Effects of patchy stomatal closure on gas exchange measurements following abscisic acid treatment. *Plant Cell Environ.* 18: 1291–1300.

Müller, P., Li, X.P. and Niyogi, K.K. (2001) Non-photochemical quenching: a response to excess light energy. *Plant Physiol.* 125: 1558–1566.

Omasa, K. (1990) Image instrumentation methods of plant analysis. *In* Physical Methods in Plant Sciences. Edited by Linskens, H.F. and Jackson, J.F. pp. 203–243. Springer-Verlag, Berlin.

Omasa, K., Abo, F., Aiga, I. and Hashimoto, Y. (1981a) Image instrumentation of plants exposed to air pollutants: quantification of physiological information included in thermal infrared images. *Trans. Soc. Instrum. Control Eng.* 17: 657–663.

Omasa, K., Abo, F., Hashimoto, Y. and Aiga, I. (1980) Measurement of the thermal pattern of plant leaves under fumigation with air pollutant. *Res. Rep. Natl. Inst. Environ. Stud. Jpn.* 11: 239–247.

Omasa, K. and Aiga, I. (1987) Environmental measurements: image instrumentation for evaluating pollution effects on plants. *In* Systems and Control Encyclopedia. Edited by Singh, M.G. pp. 1516–1522. Pergamon, Oxford.

Omasa, K. and Croxdale, J.G. (1992) Image analysis of stomatal movements and gas exchange. *In* Image Analysis in Biology. Edited by Häder, D.P. pp. 171–193. CRC Press, Boca Raton.

Omasa, K., Hashimoto, Y. and Aiga, I. (1981b) A quantitative analysis of the relationships between SO_2 or NO_2 sorption and their acute effects on plant leaves using image instrumentation. *Environ. Cont. Biol.* 19: 59–67.

Omasa, K., Hashimoto, Y. and Aiga, I. (1981c) A quantitative analysis of the relationships between O_3 sorption and its acute effects on plant leaves using image instrumentation. *Environ. Cont. Biol.* 19: 85–92.

Omasa, K., Hashimoto, Y. and Aiga, I. (1983) Observation of stomatal movements of intact plants using an image instrumentation system with a light microscope. *Plant Cell Physiol.* 24: 281–288.

Omasa, K., Hashimoto, Y., Kramer, P.J., Strain, B., Aiga, I. and Kondo, J. (1985) Direct observation of reversible and irreversible stomatal responses of attached sunflower leaves to SO_2. *Plant Physiol.* 79: 153–158.

Omasa, K., Saji, H., Youssefian, S. and Kondo, N. (2002) *Air Pollution and Plant Biotechnology. Prospects for Phytomonitoring and Phytoremediation*. pp. 155–178, 287–359. Springer, Tokyo.

Omasa, K., Shimazaki, K., Aiga, I., Larcher, W. and Onoe, M. (1987) Image analysis of chlorophyll fluorescence transients for diagnosing the photosynthetic system of attached leaves. *Plant Physiol.* 84: 748–752.

Ort, D.R. (2001) When there is too much light. *Plant Physiol.* 125: 29–32.

Ort, D.R. and Baker, N.R. (2002) A photoprotective role for O_2 as an alternative electron sink in photosynthesis? *Curr. Opin. Plant Biol.* 5: 193–198.

Osmond, C.B. (1981) Photorespiration and photoinhibition: some implications for the energetics of photosynthesis. *Biochim. Biophys. Acta* 639: 77–98.

Osmond, C.B., Daley, P.F., Badger, M.R. and Lüttge, U. (1998) Chlorophyll fluorescence quenching during photosynthetic induction in leaves of *Abutilon striatum* Dicks. infected with Abutilon mosaic virus, observed with a field-portable imaging system. *Bot. Acta* 111: 390–397.

Raskin, I. and Ladyman, J.A.R. (1988) Isolation and characterization of a barley mutant with abscisic-acid-insensitive stomata. *Planta* 173: 73–78.

Rolfe, S.A. and Scholes, J.D. (1995) Quantitative imaging of chlorophyll fluorescence. *New Phytol.* 131: 69–79.

Schreiber, U. and Neubauer, C. (1990) O_2-dependent electron flow, membrane energization and the mechanism of non-photochemical quenching of chlorophyll fluorescence. *Photosynth. Res.* 25: 279–293.

Sharkey, T.D., Berry, J.A. and Sage, R.F. (1988) Regulation of photosynthetic electron-transport in *Phaseolus vulgaris* L., as determined by room-temperature chlorophyll *a* fluorescence. *Planta* 176: 415–424.

Siebke, K. and Weis, E. (1995) Assimilation images of leaves of *Glechoma hederacea*: analysis of non-synchronous stomata related oscillations. *Planta* 196: 155–165.

Taconet, O., Olioso, A., Ben, Mehrez, M. and Brisson, N. (1995) Seasonal estimation of evaporation and stomatal conductance over a soybean field using surface IR temperatures. *Agr. Forest Meteorol.* 73: 321–337.

Terashima, I. (1992) Anatomy of non-uniform leaf photosynthesis. *Photosynth. Res.* 31: 195–212.

Terashima, I., Wong, S.C., Osmond, C.B. and Farquhar, G.D. (1988) Characterisation of non-uniform photosynthesis induced by abscisic acid in leaves having different mesophyll anatomies. *Plant Cell Physiol.* 29: 358–394.

(Received May 10, 2003; accepted September 2, 2003)